Vector Control of the Single-Phase Inverter Based on the Extended and Virtual Circuits

Tao Xu, Ming Yang, Naizhe Diao, Xianrui Sun, Suliang Wu, Zhuangzhuang Shen, Hongzhi Chen, and Chonghui Song

***Abstract*—A vector control based on the extended equivalent circuit and virtual circuits is proposed for the single-phase inverter. By the extended circuit, the other two phase voltages can be extended by the output voltage of the single-phase inverter so as to construct the voltage vector. The voltage outer-loop is to control the voltage vector in *dq* coordinate system, and the output voltage can track the target value without deviation in steady state. By designing the virtual circuit, the voltage inner-loop can achieve approximate decoupling and improve the dynamic response under the changeable load. Compared with the traditional dual closed-loop control, the proposed dual closed-loop control scheme only needs to detect and control the voltage without the current. It not only can achieve good control effect, but also reduce the complexity of the hardware. Finally, the simulation and experimental results show that the single-phase inverter has good static and dynamic characteristics regardless of stable load or changeable load.**

***Index Terms*—Coordinate transformation, dual closed-loop control; extended circuit, single-phase inverter, vector control; virtual circuit.**

I. INTRODUCTION

THAT the output voltage can quickly track the desired value is an important criterion for the single-phase inverter. A good inverter requires a good static response and fast dynamic response. Besides, it needs a hard output characteristic and a good robustness when a load changes frequently. For a single-phase inverter, the deviation based closed-loop control is widely used. The control schemes based on the traditional closed-loop control can be roughly summarized as follows: (i) the voltage and current dual closed-loop control [1-3], (ii) the voltage and current's eigenvalue feedback control [4-5], (iii) the output feedforward on a closed-loop control [6-8], (iv) the advanced control algorithm [9-10], (v) the virtual impedance technique as a auxiliary measure of variable feedback control [11-12]. The voltage and current dual closed-loop control is difficult to eliminate steady-state error. The eigenvalue feedback control can eliminate steady-state error, but it can increase the adjustment time. The output feedforward can improve dynamic performances, whereas it makes the adjustment time increase. Although using advanced control algorithm can improve the dynamic and static performances of the inverter, it increases the complexity of the controller and the debugging difficulty. The virtual impedance technique makes performances of the inverter further improved, but it still retains the shortcomings of traditional closed-loop control.

In this paper, a vector control based on the extended equivalent circuit and virtual circuits is proposed for the single-phase inverter. By the extended circuit, the other two phase voltages can be extended by the output voltage of the inverter so as to construct the voltage vector. The voltage outer-loop is to control the voltage vector in dq coordinate system, and the output voltage can track the target value without deviation in steady state. By designing the virtual circuit, the voltage inner-loop can achieve approximate decoupling and improve the dynamic response under the changeable load. Compared with the traditional dual closed-loop control, the proposed dual closed-loop control scheme only needs to detect and control the voltage without the current. It not only can achieve good control effect, but also reduce the complexity of the hardware. Finally, the simulation and experimental results show that the single-phase inverter has good static and dynamic characteristics regardless of stable load or changeable load.

II. ANALYSIS OF THE SINGLE-PHASE INVERTER

A. Control Principle of the Single-phase Inverter

The single-phase inverter [13-15] consists of the H-bridge circuit and *LC* filter circuit. The circuit diagram is shown in Fig. 1. *L* is the filter inductance and *C* is the filter capacitor. S_1, S_2, S_3 and S_4 are Insulated Gate Bipolar Transistors, i.e., IGBT. D_1, D_2, D_3 and D_4 are freewheeling diodes. V_{DC} and u_{inPWM} are the *DC*-link voltage of inverter and the output square wave voltage of the H-bridge. u_L , u_o , and Z_L are the voltage across the inductor, the output voltage of the inverter and the load impedance, respectively.

Assuming that the harmonic component of u_{inPWM} can be filtered by the *LC* filter, the H-bridge can be equivalent to a controlled AC voltage source, i.e., u_{in} . The equivalent circuit of the single-phase inverter is shown in Fig. 2.

Manuscript was submitted for review on 31, January, 2018.

This work was supported in part by the National Natural Science Foundation of China under Grant 61773006. The authors are with the Department of Information Science & Engineering, Northeastern University(email: chonghui.song@gmail.com, fightingdays@outlook.com).

Digital Object Identifier 10.30941/CESTEMS.2018.00040

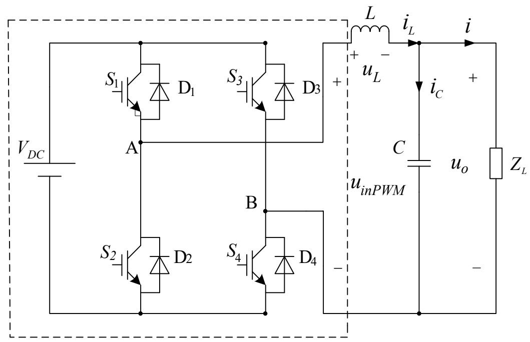

Fig. 1. The circuit diagram of the signal-phase inverter

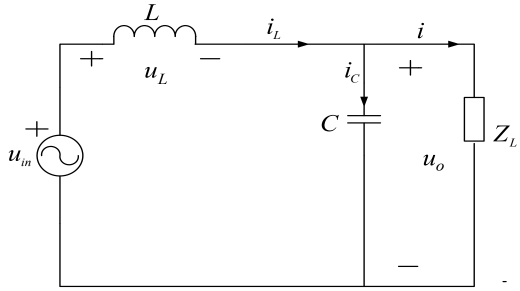

Fig. 2. The equivalent circuit of the single-phase inverter.

From the equivalent circuit, the relationship of the input voltage and output voltage is

$$u_{in} = LC\frac{d^2u_o}{dt^2} + \frac{L}{R}\frac{du_o}{dt} + u_o \,. \tag{1}$$

The phasor relationship between these physical quantities is shown in Fig. 3.

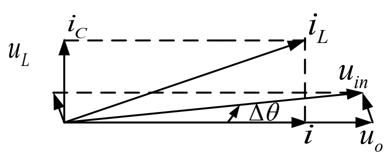

Fig. 3. Phasor diagram of equivalent circuit.

Because of the filter inductance, u_o lags behind u_{in} at an angle of $\Delta\theta$. Besides, since u_L is far less than u_o, $\Delta\theta$ is very small and the amplitudes of u_o and u_{in} are approximately equal. $\Delta\theta$ depends on the characteristic and size of the load, so $\Delta\theta$ is unknown due to unknown load. In this paper, the resistive load is taken as an example without special instructions. Thus, $\Delta\theta$ is more than zero.

The control target of the single-phase inverter is that u_o is equal to the desired voltage u_o^*. Here, u_o^* is

$$u_o^* = U^* \, cos(\omega t) \,. \tag{2}$$

From Fig. 3, when the inverter output voltage is equal to the desired voltage, the fundamental component of the input voltage should be

$$u_{in}^* = (U^* + \Delta U^*)\, cos(\omega t + \Delta\theta^*) \tag{3}$$

where ΔU^* is the amplitude increment, and $\Delta\theta^*$ is the phase increment. Assume that the input voltage of the equivalent circuit is

$$u_{in} = U_{in}\cos(\omega t + \theta + \Delta\theta) \tag{4}$$

where U_{in} is the magnitude of the input voltage, and $\theta+\Delta\theta$ is the initial angle. At the time, the corresponding output voltage is

$$u_o = U\cos(\omega t + \theta) \tag{5}$$

where U is the magnitude of the output voltage u_o, and θ is the initial angle. The basic control principles of the inverter are that U_{in} is equal to $U^* + \Delta U^*$ and that is equal to $\Delta\theta^*$. Therefore, it can be ensured that u_o is entirely equal to u_o^*.

B. Three-phase Extended Circuit and Construction of Space Vector

For a closed-loop control based on the stationary coordinate system, using a typical PI regulator cannot achieve the output voltage track the desired voltage without deviation in steady state. For a closed-loop control based on the synchronous rotating coordinate system, the coordinate transformation is mainly used to transform the AC quantities of the stationary coordinate system into the DC quantities of the synchronous rotating coordinate system, so a typical PI regulator can be used to realize the output voltage track the desired voltage without deviation.

The equivalent circuit of the single-phase inverter can be seen as a one-phase loop of a three-phase inverter. In turn, the single-phase circuit can generate the other two phase so that the equivalent circuit of three-phase extension is gotten. The extended circuit is shown in Fig. 4. The three phase voltages are u_a, u_b and u_c, where $u_a = u_o$. In the three-phase extended circuit, each phase amplitudes of the three phase input voltages are equal while the phase difference is *120°*. Each phase inductance, filter capacitance and load are also equal, respectively. Each phase amplitudes of the output voltages are the same and the phase difference is *120°*. The *a*-phase of the three-phase extended circuit is equivalent to the equivalent circuit of the single-phase inverter. Thus, the voltage vector can be constructed by the voltages of the three-phase extended equivalent circuit.

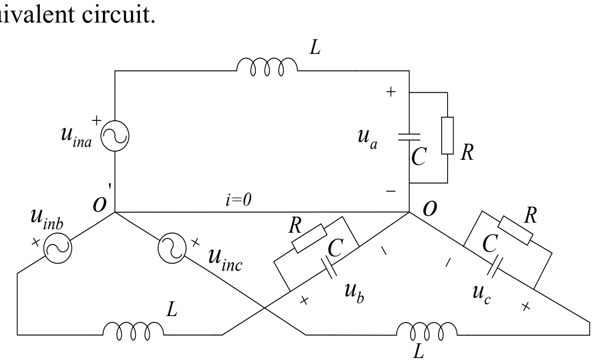

Fig. 4. Three-phase extended equivalent circuit.

The output voltages u_a, u_b and u_c of the three-phase extended equivalent circuit can construct the voltage vector $\vec{u}_o$. The voltage vector can be decomposed into $u_{o\alpha}$ and $u_{o\beta}$ in $\alpha\beta$ coordinate system, where $u_{o\alpha}$ is the α-axis component and

$u_{o\beta}$ is the β-axis component. Because only the single-phase voltage u_o can be measured and $u_{o\alpha}$, u_a and u_o are equal, $u_{o\beta}$ can be generated by FFT. The two components synthesize the vector $\vec{u}_o$ whose synthesis is shown in Fig. 5. Black lines represent *abc* coordinate system, green lines represent $\alpha\beta$ coordinate system, and the red line represents the voltage vector.

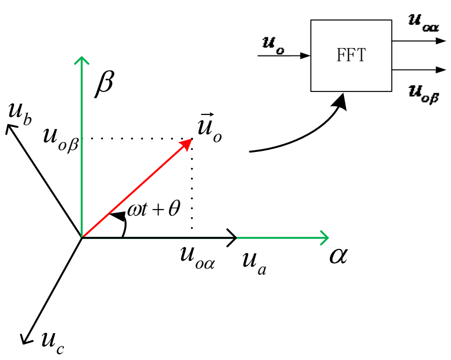

Fig. 5. Synthetic space vector.

The input equation of Fourier transformation is

$$u_o = U\cos(\omega t+\theta)\,. \tag{6}$$

The output equation of Fourier transformation is

$$\begin{cases} \vec{u}_o = u_{o\alpha} + ju_{o\beta} \\ u_{o\alpha} = FFT(u_o)_\alpha = U\cos(\omega t+\theta) \\ u_{o\beta} = FFT(u_o)_\beta = U\sin(\omega t+\theta) \end{cases} \tag{7}$$

C. The Relationship between Space Vectors

$u_{o\alpha}$ and $u_{o\beta}$ are transformed into u_{od} and u_{oq} in *dq* coordinate system by Park transformation. The relationship between the output voltage vector $\vec{u}_{in}$ of the H bridge and the output voltage vector $\vec{u}_o$ of the inverter is shown in Fig. 6. The black lines represent the stationary coordinate system, the green lines represent *dq* coordinate system, and the blue lines represent the voltage vector.

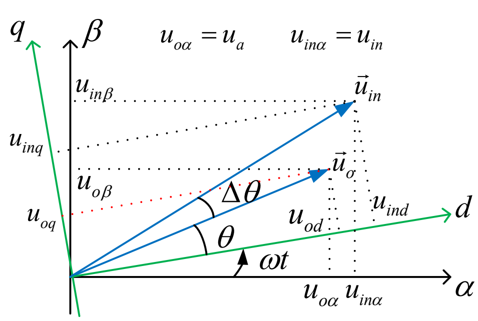

Fig. 6. The vector diagram of *dq* coordinate system.

In the figure, u_{od} and u_{oq} are the components of $\vec{u}_o$ in *dq* coordinate system. Similarly, $u_{in\alpha}$ and $u_{in\beta}$ are the components of $\vec{u}_{in}$ in $\alpha\beta$ coordinate system. u_{ind} and u_{inq} are the components of $\vec{u}_{in}$ in *dq* coordinate system.

III. Design of Dual Closed-loop Controller For The Inverter

To reduce the complexity of the hardware and realize the output voltage track the desired voltage without static difference, Based on the voltage vector and virtual circuit, the voltage dual closed-loop control can be used. The voltage outer-loop is to control the voltage vector in *dq* coordinate system, and the output voltage can track the desired value without deviation in steady state. The voltage inner-loop is to achieve approximate decoupling and improve the dynamic response by designing the virtual circuit.

A. The Design of Voltage Outer-loop

Assuming that u_{in}^* is the input of meeting $u_o = u_o^*$, the vector relationship is shown in Fig. 7. The red lines represent the desired voltage vectors $\vec{u}_{in}^*$ and $\vec{u}_o^*$. $\vec{u}_{in}^*$ is a synthetic vector by the three phase extension. $\vec{u}_o^*$ is also a synthetic vector on d-axis. If the α-axis component $u_{in\alpha}^*$ of $\vec{u}_{in}^*$ is a modulated signal, the output of the single-phase inverter is u_o^*. When the amplitude $U^*+\Delta U^*$ and the phase angle $\omega t+\Delta\theta^*$ of u_{in}^* vary with the load, the closed-loop control can make u_{in} tend to u_{in}^*. The vector relationship is shown in Fig. 8. The red lines represent the desired voltage vector $\vec{u}_{in}^*$ and $\vec{u}_o^*$. The blue lines represent the transient voltage vector $\vec{u}_{in}$ and $\vec{u}_o$ in the dynamic process. The components of $\vec{u}_o$ in *dq* coordinate system and the desired value are given to the PI so that $\vec{u}_o$ approaches $\vec{u}_o^*$. When the steady state is reached, u_{in} is equal to u_{in}^* and u_o is equal to u_o^*.

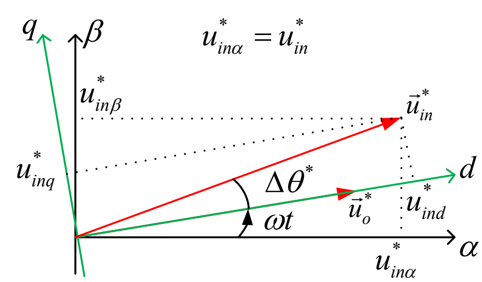

Fig. 7. The vector diagram of the open-loop control.

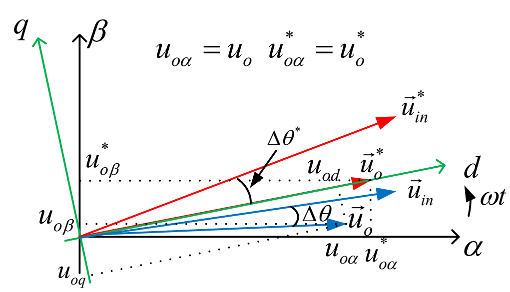

Fig. 8. The vector diagram of the closed-loop control.

$\vec{u}_{in}$ and $\vec{u}_o$ can be expressed as $\vec{u}_{in} = u_{in\alpha} + ju_{in\beta}$ and $\vec{u}_o = u_{o\alpha} + ju_{o\beta}$ in $\alpha\beta$ coordinate system. (1) in $\alpha\beta$ coordinate system is expressed as

$$\vec{u}_{in} = LC\frac{d^2\vec{u}_o}{dt^2} + \frac{L}{R}\frac{d\vec{u}_o}{dt} + \vec{u}_o \,. \tag{8}$$

$\vec{u}_{in}$ and $\vec{u}_o$ can be expressed as $\vec{u}_{in} = u_{ind} + ju_{inq}$ and $\vec{u}_o = u_{od} + ju_{oq}$ in dq coordinate system. Then (8) can be further transformed into (9) in dq coordinate system.

$$e^{j\theta}\vec{u}_{in} = LC\frac{d^2 e^{j\theta}\vec{u}_o}{dt^2} + \frac{L}{R}\frac{de^{j\theta}\vec{u}_o}{dt} + e^{j\theta}\vec{u}_o \tag{9}$$

where $e^{j\theta}$ is the introduced rotating factor. The transfer function of (9) can also be written in the form of a matrix shown in (10), and the structure of the control object is shown in Fig. 9.

$$\begin{bmatrix} u_{ind}(s) \\ u_{inq}(s) \end{bmatrix} = A\begin{bmatrix} u_{od}(s) \\ u_{oq}(s) \end{bmatrix} + B\begin{bmatrix} i_d(s) \\ i_q(s) \end{bmatrix} \tag{10}$$

where A is $\begin{bmatrix} LCs^2+1-LC\omega^2 & -2LC\omega s \\ 2LC\omega s & LCs^2+1-LC\omega^2 \end{bmatrix}$ and B is $\begin{bmatrix} Ls & -\omega L \\ \omega L & Ls \end{bmatrix}$.

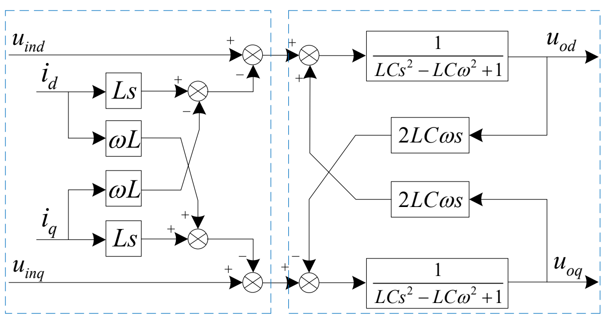

Fig. 9. The mathematical model of the single-phase inverter.

From (10) and Fig. 9, u_{ind}, u_{inq}, u_{od} and u_{oq} have coupling relationships and i_d and i_q also have coupling relationships. To achieve decoupling, a feedforward decoupling strategy is taken, but increasing the feedback of the output current needs current sensors and current detection circuit so that the hardware is complex. In these coupling items and the forward transfer function, it is seen that L determines the strength of these coupling items and the influence of the output current on the input voltage. The approximate decoupling can be achieved if L is greatly reduced. Thus, in the design of the outer-loop, these relationships can be neglected between voltage and current including $2LC\omega s$, ωL and Ls. Instead, designing the inner-loop reduces the above effect. (10) can be simplified into

$$\begin{bmatrix} u_{ind}(s) \\ u_{inq}(s) \end{bmatrix} = \bar{A}\begin{bmatrix} u_{od}(s) \\ u_{oq}(s) \end{bmatrix} \tag{11}$$

where $\bar{A}$ is $\begin{bmatrix} LCs^2+1-LC\omega^2 & 0 \\ 0 & LCs^2+1-LC\omega^2 \end{bmatrix}$.

Since the components of the voltage vector in dq coordinate system are the DC quantities, the general PI regulator can be used. The voltage control equation is expressed as

$$\begin{cases} u_{ind}(s) = (k_{P1} + \dfrac{k_{I1}}{s})(u_{od}^*(s) - u_{od}(s)) \\ u_{inq}(s) = (k_{P1} + \dfrac{k_{I1}}{s})(u_{oq}^*(s) - u_{oq}(s)) \end{cases} . \tag{12}$$

The outer-loop control block diagram is shown in Fig. 10. The red solid line frame is the PI feedforward control section of the voltage outer-loop and the red dashed box is a conventional decoupling control.

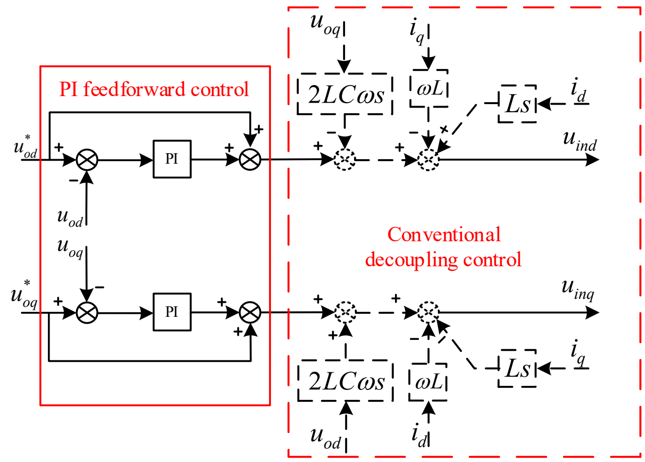

Fig. 10. The block diagram of the outer-loop control.

B. The Design of Voltage Inner-loop

From Fig. 9, the coupling factor of u_{ind}, u_{inq} and u_{od}, u_{oq} is ωLC, and the coupling factor of i_d and i_q is ωL. Besides, the forward transfer function of u_{ind}, u_{inq} affected by i_d, i_q is Ls. The value of inductance determines the strength of the coupling and the influence of i_d and i_q on the modulated voltage u_{in}. When the load changes, the freewheeling effect of the inductor causes the capacitor current to fluctuate, so that the output voltage has a big fluctuation. In particular, when the load is a diode load, only the voltage outer-loop cannot correct the deviation of the output voltage in the half cycle. To reduce the coupling relationship and decrease the direct influence of dq-axis current, and improve the dynamic response speed of the output voltage, the inner-loop controller based on the virtual impedance is designed.

When the load suddenly disconnect, the output voltage becomes larger and its phase is behind the desired voltage at an angle of θ due to the suppression of the inductor on the current. The vector relationships are shown in Fig. 11.

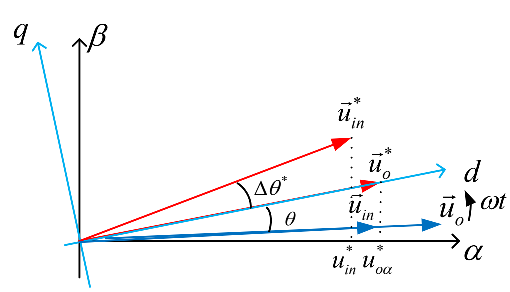

Fig. 11. The vector diagram of the inner-loop control after the load is disconnected

The controller is designed shown in Fig. 12. The red dashed box is the transfer function of the original system, and the red solid frame is the transfer function of the new system.

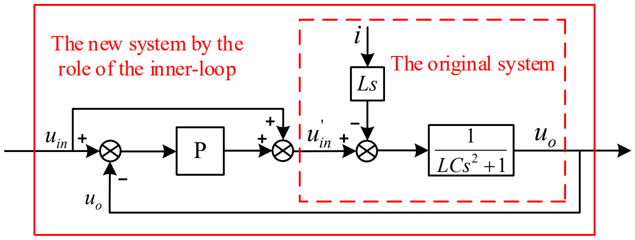

Fig. 12. The block diagram of the inner-loop control

As the load is unknown, the original system can be seen as a controlled voltage source. Its transfer function is expressed as

$$U_{in}(s)=(LCs^2+1)U_o(s)+LsI(s). \tag{13}$$

When the inner-loop is a P controller, combining the original system with the controller is seen as a new system. The open-loop transfer function of the new system is

$$U_{in}(s)=(\bar{L}Cs^2+1)U_o(s)+\bar{L}sI(s) \tag{14}$$

where $\bar{L}=L/(1+K_{P3})$. K_{P3} is the inner-loop proportional coefficient.

From the perspective of the circuit, the equivalent virtual circuit is suitable for the low-frequency range far below the carrier frequency of the PWM signal. The harmonics near the fundamental frequency and below the fundamental frequency have a great influence on the output voltage waveform. The larger the $\bar{L}$ is, the better the effect of suppressing these harmonics is, so K_{P3} cannot be too large.

After adding the P controller, the new system can be equivalent to be shown in Fig. 13. The filter inductance is reduced to $1/(1+K_{P3})$ of the original, so the voltage and current of the *dq*-axis are approximately decoupled. In addition, when the load changes, the effect of inductance on current is reduced to make the output voltage quickly track the desired voltage. In summary, the inner-loop control is to achieve the approximate decoupling and speed up the dynamic response.

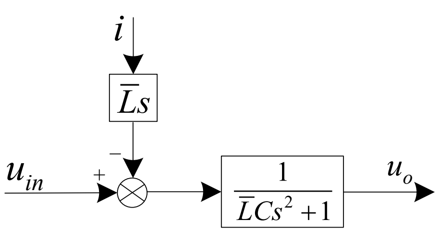

Fig. 13. The equivalent structure of the new system after adding the inner-loop.

C. System Control Structure Block Diagram

The overall block diagram of the system control is shown in Fig. 14. The detected output voltage u_o is taken Fourier transformation to obtain the voltages $u_{o\alpha}$ and $u_{o\beta}$ in $\alpha\beta$ coordinate system. By $\alpha\beta$ to dq transformation, $u_{o\alpha}$ and $u_{o\beta}$ are transformed into u_{od} and u_{oq}. Firstly, the outer-loop PI controllers regulate u_{od} and u_{oq}, respectively. The output of the outer-loop PI regulator is transformed into the voltage u_{in} which is the α-axis voltage. Secondly, u_{in} is regulated by the P regulator of the inner-loop. The output of the P controller is the modulation voltage u_{in}'. Finally, the modulation voltage controls the power module to output a AC voltage through SPWM method, and the AC voltage adjusts the output voltage u_o of the single-phase inverter.

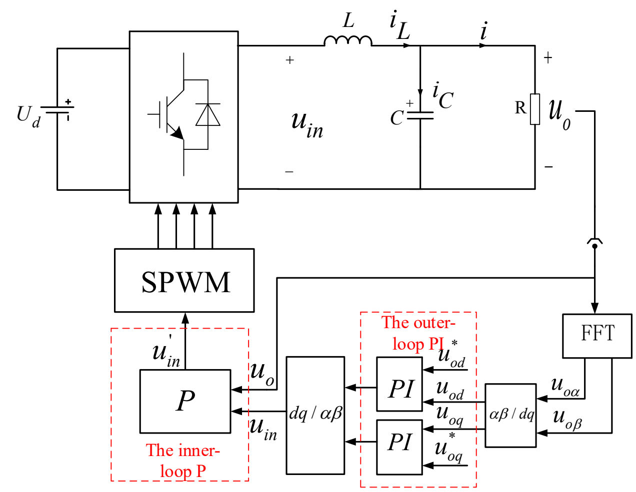

Fig. 14. The system control block diagram.

IV. Simulation And Experimental Results Analysis

To test and verify the dual closed-loop control scheme of the single-phase inverter based on the extended and virtual circuit, the models developed above are implemented in both computer simulations and the experimental hardware. The results are given below.

A. Simulation of PLECS and Analysis of Results

5kVA single-phase inverter is simulated in the time domain with programs written in PLECS. The simulation parameters of the system are as follows. The output voltage is 220V/50Hz. The DC-link voltage is 311V. The inductance is 2.2mH. The capacitance is $50uF$ and the triangular carrier frequency is 8kHz. Besides, parameters of the outer-loop PI regulator are $K_{P1}=1.75$, $K_{I1}=20$, $K_{P2}=1.75$ and $K_{I2}=20$, and the parameter of the inner-loop PI regulator is $K_{P3}=10.34$. The full load (R=10Ω) and the diode rectifier load (a diode in series with a 10Ω resistor) for the single-phase inverter are verified, respectively.

The voltage and current dual closed-loop controller and voltage dual closed-loop controller are simulated for its response to a full step load and the step time is 1.025s. The results are shown in Fig. 15. It can be seen from Fig. 15 that both controllers exhibit a similar "notch" in the output voltage. Considering the steady state though, it can be clearly seen that the voltage and current dual closed-loop controller exhibits a prominent "AC following error" while the voltage dual closed-loop controller regulates this error to zero in less that 1/6 cycle of the AC voltage.

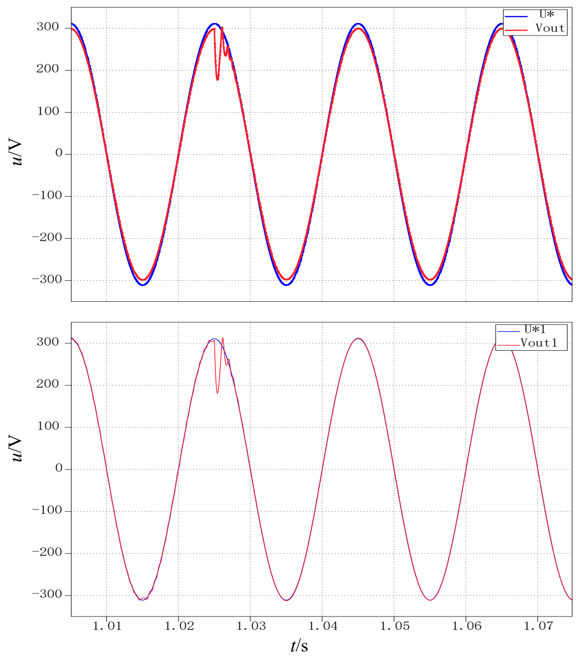

Fig. 15. Simulation waveform comparison of voltage and current dual closed-loop (Top) and voltage dual closed-loop (Lower).

Fig. 16 shows the output voltage and output current waveform of the inverter with the diode rectifier load. When the diode load is on, it is equivalent to the full load. When the diode load is off, the system is no-load. From the figure, the output voltage of the inverter can still track the desired voltage.

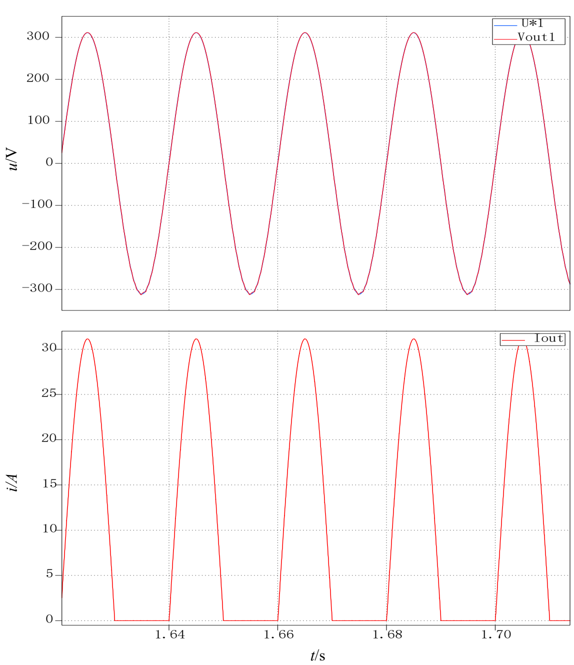

Fig. 16. The output voltage and current waveform with the diode load.

B. *Experiment and Result Analysis*

The system uses Field Programmable Gate Array, i.e, FPGA, as the core to achieve the vector control of full bridge inverter, and the internal IP core to achieve FFT. Using the proposed control strategy builds the experimental platform. The experimental parameters are shown in Table 1.

TABLE I
THE EXPERIMENTAL PARAMETERS OF THE MAIN CIRCUIT

Parameter	Quantity
DC-link voltage V_{dc}/V	48
AC filter capacitor C/uF	50
AC filter inductance L/mH	2.2
Load Resistance R_L/Ω	9
Switching frequency f_s/kHz	8
Output AC line voltage U_o/V	26
Output AC voltage frequency f/Hz	50

The experimental platform is shown in Fig.17.

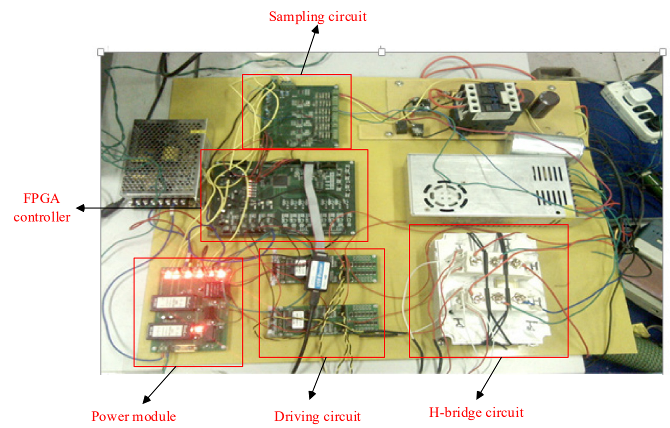

Fig. 17. Experiment platform.

Fig. 18 shows the output voltage waveform when the inverter is no-load. Fig. 19 shows the output voltage waveform under the linear load condition. Fig. 20 shows the output voltage waveform of the inverter under the rectifier load. Fig. 21 is the voltage waveform across the resistor of the rectifier load. Because the load is purely resistive load, the current waveform through the resistor is consistent with the voltage waveform across the resistor.

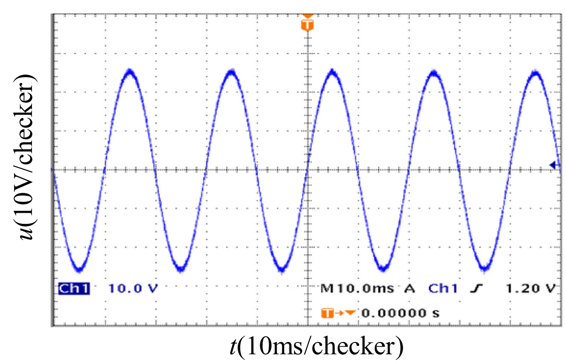

Fig. 18. No-load inverter output voltage waveform.

It can be seen from Fig. 18, Fig. 19, Fig. 20 and Fig. 21 that the experimental results are basically consistent with the simulation results. It indicates that the control strategy proposed in this paper can make the output voltage accurately track the desired voltage. When the load is a diode load, the system still responds very quickly.

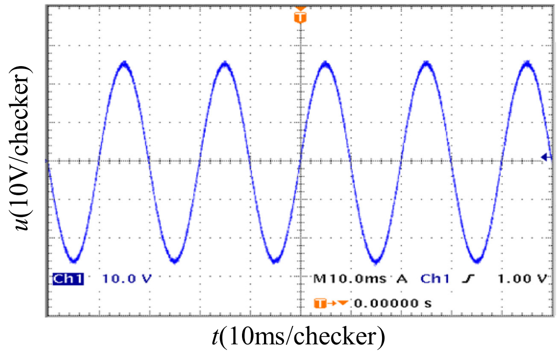

Fig. 19. Full-load inverter output voltage waveform.

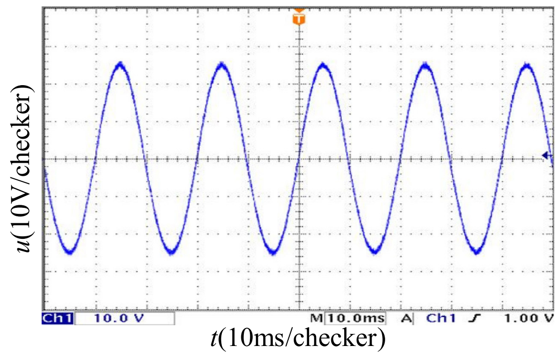

Fig. 20. The output voltage waveform for rectifier load.

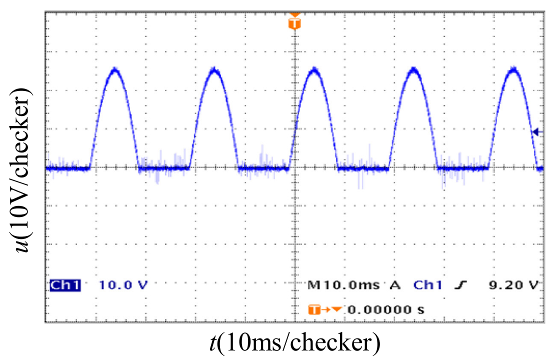

Fig. 21. The voltage waveform across the resistor of the rectifier load.

V. Conclusion

In this paper, the single-phase full-bridge inverter is researched, and the dual closed-loop vector control of the single-phase inverter is proposed. The method of the three-phase extended circuit is given, and the single-phase inverter circuit is extended into the three-phase equivalent circuit. Thus, the vector control of the three-phase circuit can be applied to the single-phase circuit. The voltage outer-loop is to control the voltage vector in *dq* coordinate system. By designing the virtual circuit, the voltage inner-loop can achieve approximate decoupling and improve the dynamic response of the system.

Compared with the traditional dual closed-loop control, the voltage dual closed-loop control only needs the feedback of the output voltage, and does not need the feedback of the current. Thus, its hardware only needs voltage sensors, the corresponding detected circuit and a simple over-current protected circuit. In other words, the voltage dual closed-loop control strategy can reduce the complexity of the hardware.

The system simulation and experimental results show that the control strategy proposed in this paper is effective. Through the dual closed-loop voltage control of the single-phase inverter, the output accuracy and response speed of the inverter are greatly improved.

References

[1] Loh P C, Newman M J, Zmood D N, et al, "Improved transient and steady state voltage regulation for single and three phase uninterruptible power supplies," in *IEEE-PESC*, Vancouver, 2001.

[2] Mihalache L, "DSP control method of single-phase inverters for UPS applications," in *Proceeding of the 26th Chinese Control Conference*, China, 2007.

[3] Cai Kun, Li Yaohua, Shen Xiaosong, et al, "Output control of the high performance single-phase voltage-source inverters," *Transactions of China Electrotechnical Society*, vol. 20, no. 1, pp. 105-107, 2005.

[4] Li Chen, Li Minyuan, Ji Shiming, et al, "Novel multiple-loop control system for 400 Hz inverter," *Proceedings of the CSEE*, vol. 30, no. 36, pp. 71-78, 2010.

[5] Li C, Ji S, Tan D, "Multiple-loop digital control method for a 400 Hz system based on phase feedback," *IEEE Transactions on Power Electronics*, vol. 28, no. 1, pp. 408-417, 2013.

[6] Fang Tianzhi, Ruan Xinbo, Xiao Lan, et al, "An improved distributed control strategy of parallel inverters," *Proceedings of the CSEE*, vol. 28, no. 33, pp. 30-36, 2008.

[7] Shen G, Xu D, Cao L, et al, "An improved control strategy for grid-connected voltage source inverters with an LCL filter," *IEEE Transactions on Power Electronics*, vol. 23, no. 4, pp. 1899-1906, 2008.

[8] Wang X, Ruan X, Liu S, et al, "Full feed forward of grid voltage for grid-connected inverter with LCL filter to suppress current distortion due to grid voltage harmonics," *IEEE Transactions on Power Electronics*, vol. 25, no. 12, pp. 3119-3127, 2010.

[9] Tang Shiying, Peng Li, Kang Yong, et al, "Research on dual-loop digital control technique for pulse width modulation inverters," *Proceedings of the CSEE*, vol. 29, no. 15, pp. 55-60, 2009.

[10] Fang Zhijian, Duan Shanxu, Chen Tianjin, et al, "Mechanism and suppression strategy of prediction control error applied in a battery energy storage inverter," *Proceedings of the CSEE*, vol. 33, no. 30, pp. 1-9, 2013.

[11] He J, Li Y, "Generalized closed-loop control schemes with embedded virtual impedances for voltage source converters with LC or LCL filters," *IEEE Transactions on Power Electronics*, vol. 27, no. 4, pp. 1850-1861, 2012.

[12] Zhang Y, Yu M, Liu F, et al, "Instantaneous current-sharing control strategy for parallel operation of UPS modules using virtual impedance," *IEEE Transactions on Power Electronics*, vol. 28, no. 1, pp. 432-440, 2013.

[13] Ryan M J, Brumsickle W E, Lorenz R D, "Control topology options for single-phase UPS inverters," *IEEE Transaction on Industry Application*, vol. 33, no. 2, pp. 493-501, 1997.

[14] Chen Juan, He Yingjie, Wang Xinyu, Liu Jinjun, "Study three-level space vector modulation strategy unified theory," *Proceedings of the CSEE*, vol. 33, no. 9, pp. 3-5, 2013.

[15] Guo Weinong, Chen Jian, "Study on digital dual-loop control for Inverters based on state-observer," *Proceedings of the CSEE*, vol. 22, no. 9, pp. 64-68, 2002.

[16] Chen Hongzhi, Wang Xu, Liu Jianchang, et al, "Virtual structure design for inverter power supply," *Transactions of China Electrotechnical Society*, vol. 28, no. 8, pp. 157-163, 2013.

[17] Chen Hongzhi, Wang Xu, Liu Jianchang, "Current sharing method for parallel inverters based impedance matching modular," *Proceedings of the CSEE*, vol. 32, no. 6, pp. 24-32, 2012.

Tao Xu was born in Anhui, China, in 1993. He received the B.S degree in electrical engineering and automation from the Northeast Petroleum University, Heilongjiang, China, 2016. He is currently working toward a M.S degree in electrical engineering from the Northeastern University, Shenyang, China.

Ming Yang was born in Heilongjiang, China, in 1994. He is currently working toward a M.S degree in electrical engineering from the Northeastern University, Shenyang, China. His research direction is power electronics and power transmission.

Naizhe Diao was born in Liaoning, China, in 1984. He received the M.S degree in electrical engineering from the Northeastern University, Shenyang, China. He is currently the Ph.D degree in Information Science and Engineering from the Northeastern University, Shenyang, China. His research direction is control engineering.

Xianrui Sun was born in Shandong, China, in 1989. He received the M.S degree in electrical engineering from the Northeastern University, Shenyang, China. His research direction was power electronics and power transmission.

Suliang Wu was born in Jiangsu, China, in 1991. He received the M.S degree in electrical engineering from the Northeastern University, Shenyang, China. His research direction was power electronics and power transmission.

Zhuangzhuang Shen was born in Shandong, China, in 1984. He received the M.S degree in electrical engineering from the Northeastern University, Shenyang, China. His research direction was Power System and Automation.

Hongzhi Chen received the Ph.D degree in Information Science and Engineering from the Northeastern University, Shenyang, China. He is currently working at a teacher. His research interests are complex industrial automation and power electronics and power transmission.

Chonghui Song received the B.S degree in Energy and Power Engineering from Xi'an Jiaotong University, Xian, China, and the Ph.D degree in Information Science and Engineering from the Northeastern University, Shenyang, China. His research interests are the Modern Power Electronics Technology, Motion Control Technology and Process Control technology.